Ma *et al. Cell Communication and Signaling* (2024) 22:398
https://doi.org/10.1186/s12964-024-01778-5

Cell Communication and Signaling

RESEARCH Open Access

The epithelial Na^+ channel (ENaC) in ovarian granulosa cells modulates Ca^{2+} mobilization and gonadotrophin signaling for estrogen homeostasis and female fertility

Xiyang Ma[1†], Ruiyao Xu[1†], Junjiang Chen[1,2], Shan Wang[1], Peijie Hu[1], Yong Wu[1], Yanting Que[1], Wanting Du[1], Xiaojun Cai[1], Hui Chen[1], Jinghui Guo[3], Tin Chiu Li[4] and Ye Chun Ruan[1,5*]

Abstract

Ovarian granulosa cells are essential to gonadotrophin-regulated estrogen production, female cycle maintenance and fertility. The epithelial Na^+ channel (ENaC) is associated with female fertility; however, whether and how it plays a role in ovarian cell function(s) remained unexplored. Here, we report patch-clamp and Na^+ imaging detection of ENaC expression and channel activity in both human and mouse ovarian granulosa cells, which are promoted by pituitary gonadotrophins, follicle stimulating hormone (FSH) or luteinizing hormone (LH). Cre-recombinase- and CRISPR-Cas9-based granulosa-specific knockout of ENaC α subunit (*Scnn1a*) in mice resulted in failed estrogen elevation at early estrus, reduced number of corpus luteum, abnormally extended estrus phase, reduced litter size and subfertility in adult female mice. Further analysis using technologies including RNA sequencing and Ca^{2+} imaging revealed that pharmacological inhibition, shRNA-based knockdown or the knockout of ENaC diminished spontaneous or stimulated Ca^{2+} oscillations, lowered the capacity of intracellular Ca^{2+} stores and impaired FSH/LH-stimulated transcriptome changes for estrogen production in mouse and/or human granulosa cells. Together, these results have revealed a previously undefined role of ENaC in modulating gonadotrophin signaling in granulosa cells for estrogen homeostasis and thus female fertility.

Introduction

Ovarian granulosa cells are the epithelial-like somatic cells that encase the oocyte in the follicle [1], where the oocyte develops to gain competence until released/ovulated [2, 3]. A main function of granulosa cells is to produce estrogens in response to gonadotropins from the hypothalamus-pituitary axis, which is essential to the maintenance of female cycle and fertility [4–7]. Follicle stimulating hormone (FSH), a pituitary gonadotropin, activates FSH receptors (FSHRs) in granulosa cells to promote the transcription of steroidogenic genes including CYP19A1, or aromatase, a key enzyme that catalyzes the conversion of androgens

†Xiyang Ma and Ruiyao Xu contributed equally to this work.

*Correspondence:
Ye Chun Ruan
sharon.yc.ruan@polyu.edu.hk
[1]Department of Biomedical Engineering, The Hong Kong Polytechnic University, Hong Kong SAR, China
[2]Jinan University, Guangzhou, China
[3]School of Medicine, The Chinese University of Hong Kong, Shenzhen, China
[4]Department of Obstetrics and Gynaecology, Prince of Wales Hospital, The Chinese University of Hong Kong, Hong Kong SAR, China
[5]Shenzhen Research Institute, The Hong Kong Polytechnic University, Shenzhen, China

to estrogens, driving oocyte growth and maturation [2, 3]. Accumulated estrogens mediate the feedback to the hypothalamus-pituitary to evoke the surge of luteinizing hormone (LH) [4], which in turn activates its receptor (LHCGR) in granulosa cells to trigger cascades of signaling pathways leading to ovulation and luteinization [8]. Dysfunction of granulosa cells may lead to disturbed estrogen homeostasis and account for follicle arrest, follicle apoptosis, anovulation and other ovarian disorders [3, 7, 9, 10]. In in vitro fertilization (IVF)-based assisted reproductive technology (ART), exogenous gonadotrophins are applied to maximize follicle maturation and ovulation, resulting in a high maternal estrogen level, which is reported to have adverse effects and requires careful management in ART [11, 12]. Despite such importance, the regulatory mechanisms of gonadotrophin signaling in granulosa cells are not fully understood.

Intracellular Ca^{2+} mobilization such as Ca^{2+} oscillation has been observed in human and animal granulosa cells, which is believed to play a critical role in mediating gonadotropin signaling for ovarian steroidogenesis, oocyte maturation and ovulation [13–16]. A number of Ca^{2+} or Na^+ channels important to Ca^{2+} mobilization have been reported to be expressed in human or mouse granulosa cells [17–19]. However, physiological roles of ion channels in granulosa cell functions and gonadotrophin signaling remain largely unexplored.

The epithelial Na^+ channel (ENaC), consisting of three subunits, α, β and γ encoded by human genes, *SCNN1A*, *SCNN1B* and *SCNN1G*, respectively, is best known for its role in Na^+ and water absorption in the kidney and airway epithelial cells [20]. Since the whole-body knockout of α subunit (ENaCα), the rate-limiting subunit of ENaC, led to respiration failure and neonatal death in mice [21], the definite roles of ENaC in other adult organ systems had not been clear. In the recent decades, ENaC has been related to female reproduction given that infertility or subfertility has been noted in women with pseudohypoaldosteronism type 1 (caused by loss-of-function mutation of ENaC genes) [22, 23]. We previously demonstrated in uterine/endometrial epithelial cells that the activation of ENaC triggers signaling pathways required for two important physiological events occurring in the uterus, embryo implantation and parturition [24–27]. However, whether ENaC is expressed in the ovary to regulate ovarian function(s) for female fertility remained unknown. Interestingly, women with a low Na^+ intake exhibited sporadic anovulation [28], suggesting possible association of Na^+ environment with ovarian function. In the present study, we hypothesized that ENaC might be expressed in granulosa cells to participate in ovarian functions. To test the hypothesis, we used a mouse model of granulosa-specific knockout of ENaC, a human granulosa cell line (KGN), as well as primary human granulosa cells collected during IVF, together with technologies such as Na^+ and Ca^{2+} imaging, patch-clamp, and RNA sequencing, which revealed the expression and function of ENaC in granulosa cells to modulate Ca^{2+} mobilization and gonadotrophin signaling for estrogen homeostasis, female cycle maintenance and fertility.

Results

Functional expression of ENaC in ovarian granulosa cells

Since ENaC expression in the ovary or granulosa cells had not been clear, we first performed quantitative PCR (qPCR) for ENaC genes in mouse ovarian tissues, primary mouse granulosa cultures, primary human granulosa cells (HGC) isolated from women under IVF treatment, as well as KGN, a human granulosa cell line, which detected the expression of all three subunits (Supplementary Figure S1), although the expression levels of β and γ subunits were relatively low compared to that of ENaCα. We next performed immunohistochemistry and immunofluorescence staining for ENaCα in ovarian tissues from adult female mice, which both showed ENaCα expression in the ovary (Fig. 1A). Particularly, in antral follicles, ENaCα was detected in both cumulus and mural granulosa cells, but not in theca cells (Fig. 1A). ENaCα expression was also noted in apical membranes of adjacent ovarian surface and oviduct epithelium, a typical expression patten of ENaC in epithelial tissues (Fig. 1A). We also confirmed protein expression of ENaCα in HGC and KGN cells by western blot (Fig. 1B). Since ENaCα is known to assemble in the membrane to form channel pore without β and γ subunits [29], we next tested if the detected ENaC expression could be functional as channel proteins using KGN cells. In a bath solution where most of Cl^- was substituted, a series of voltage stimulations from −100 to 0 mV elicited small inward whole-cell currents (Fig. 1C). The addition of trypsin (20 μg/mL), a serine protease known to activate ENaC, into the bath, caused substantial increasement of these currents, which were blocked by subsequent addition of amiloride (10 μM), a selective ENaC inhibitor, indicating ENaC channel activities in KGN cells (Fig. 1C). To confirm this, we next measured intracellular Na^+ levels in KGN cells using a fluorescent dye sensitive to Na^+ concentrations, SBFI. Results showed that the intracellular Na^+ level was gradually elevated by trypsin (20 μg/mL), which was bluntly decreased by subsequent addition of amiloride (1 μM) to a low level (Fig. 1D), suggesting ENaC to mediate Na^+ influx into granulosa cells. These findings collectively revealed

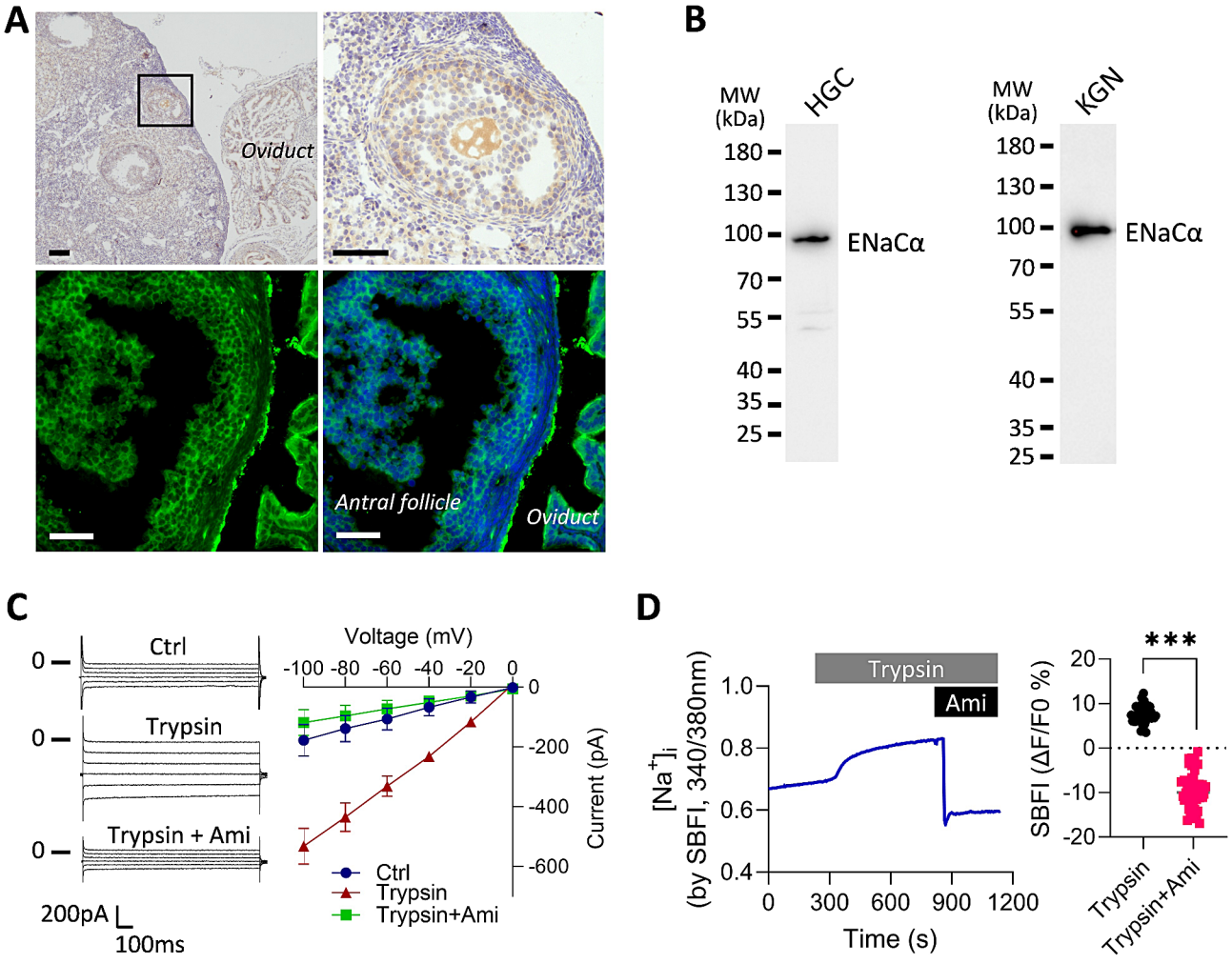

Fig. 1 Functional expression of ENaC in ovarian granulosa cells. (**A**) Immunohistochemistry and immunofluorescence staining for ENaCα in mouse ovarian tissues. Nuclei were labeled with hematoxylin or DAPI. Scale bars, 100 μm. (**B**) Western blots for ENaCα in human granulosa cells isolated from women under IVF treatment (HGCs) and in KGN, a human granulosa cell line. (**C**) Representative patch-clamp whole-cell currents elicited from − 100 to 0 mV in a KGN cell, before (Ctrl) and after the addition of trypsin (20 μg/mL), an activator of ENaC, and subsequently amiloride (Ami, 10 μM), a selective inhibitor of ENaC. Corresponding current-voltage curves are shown on the right. $n = 3$. (**D**) Representative time-course measurement of intracellular Na^+ levels ($[Na^+]_i$, indicated by 340/380 ratio of SBFI, a Na^+ sensitive fluorescent dye) in KGN cells before and after the addition of trypsin (20 μg/mL) and subsequently Ami (1 μM), with corresponding statistical analysis. $n = 43$ cells. $^{***}P < 0.001$ by Unpaired Student's t-test

ENaC to be functionally expressed in ovarian granulosa cells.

Gonadotrophins upregulate and activate ENaC in granulosa cells

We next asked if the expression level of ENaC in granulosa cells would change in the female/estrus cycle. qPCR using ovarian tissue RNAs from mice at different phases of the estrus cycle (i.e., diestrus, proestrus, estrus and metestrus) suggested similar mRNA levels of all three subunits of ENaC over different estrus phases (Supplementary Figure S1C). However, protein expression of ENaCα in the mouse ovary altered significantly in the estrus cycle with higher levels detected at proestrus and estrus, and lower at metestrus and diestrus phases (Fig. 2A). Consistent with such expression pattern, FSH and LH, the two gonadotrophins known to rise at proestrus in mice, upregulated protein expression of ENaCα in mouse granulosa cell cultures (Fig. 2B-C). Interestingly, FSH was also found to activate amiloride-sensitive ENaC currents in KGN cells (Fig. 2D). These results together suggest granulosa ENaC to be promoted by gonadotrophins.

Granulosa-cell specific knockout of ENaC disturbs estrus cycle and impairs female fertility in mice

Next, to test whether the expression of ENaC in granulosa cells is required for ovarian function(s), we built a mouse model where ENaC is conditionally knocked out in granulosa cells. Since ENaCα(*Scnn1a*) is the rate-limiting

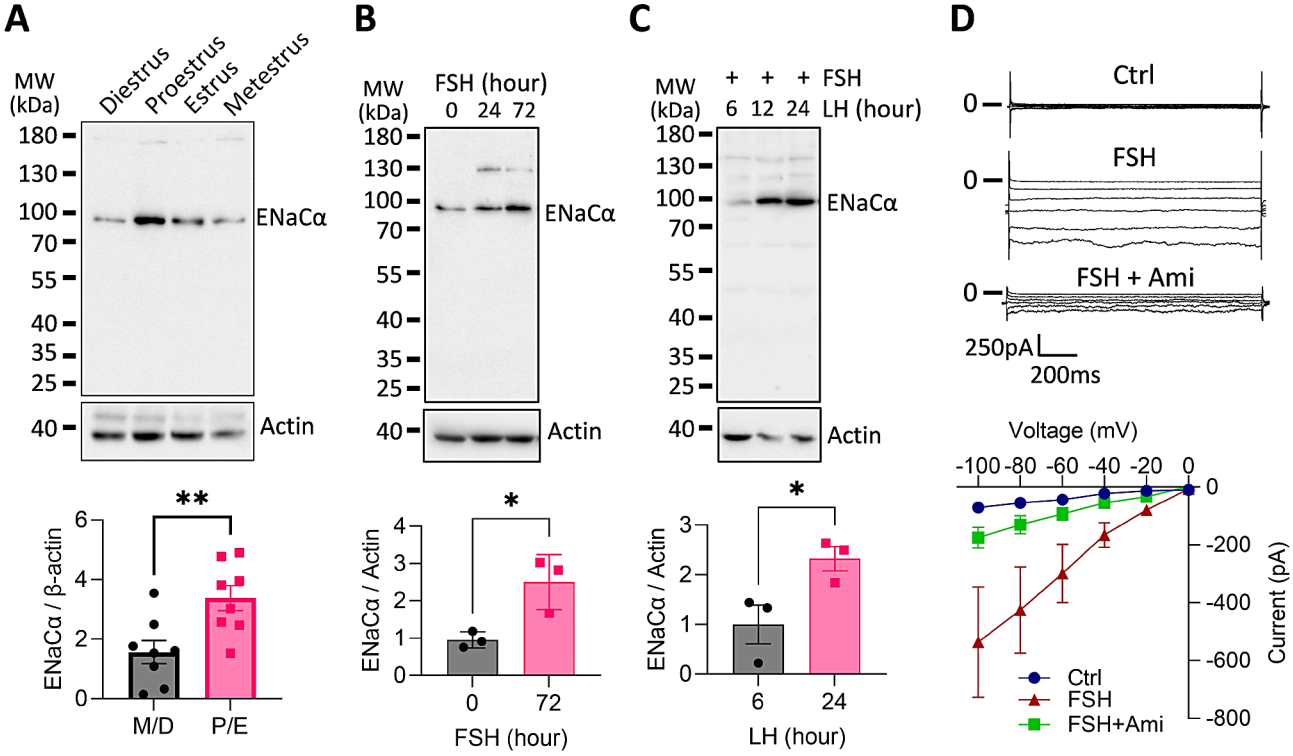

Fig. 2 Gonadotrophins upregulate and activate ENaC in granulosa cells. (**A**) Western blots for ENaCα in ovarian tissues from adult female mice at different phases of the estrus cycle (determined by daily vaginal spear, diestrus (**D**), proestrus (P), estrus (E), metestrus (M)). $n=8$. $^{**}P<0.01$ by Unpaired Student's t-test. (**B**-**C**) Western blots for ENaCα in primary cultured mouse granulosa cells before and after treated with follicle stimulating hormone (FSH, 100 ng/mL) for 0, 24, 72 h (**B**) or luteinizing hormone (LH, 100 ng/mL) for 6, 12, 24 h (**C**). Cells were pretreated with FSH (100 ng/mL) for 48 h before LH was added. $n=3$. $^{*}P<0.05$ by Unpaired Student's t-test. (**D**) Representative patch-clamp whole-cell currents elicited from − 100 to 0 mV in a KGN cell, before (Ctrl) and after the addition of FSH (100 ng/mL) and subsequently Ami (10μM), with corresponding current-voltage curves $n=3$

factor for ENaC to function, we constructed a *Scnn1a* floxed transgenic mouse line (*Scnn1a*$^{fl/fl}$) and crossed it with another line, where Cre-recombinase under the promoter of *Cyp19a1* (a granulosa-specific gene) was inserted (*Cyp19a1*^{Cre}), to generate the conditional knockout (cKO, *Scnn1a*$^{fl/fl}$*Cyp19a1*$^{Cre+}$, Supplementary Figure S2A). Immunofluorescence staining in ovarian tissues from the cKO mice showed the absence of ENaCα in the granulosa cells of the antral follicles, in comparison with Cre-negative control mice (Ctrl, *Scnn1a*$^{fl/fl}$*Cyp19a1*$^{Cre-}$) (Fig. 3A). Western blots confirmed that protein expression of ENaCα was drastically reduced in granulosa cultures from the cKO mice compared to that of the Ctrl mice (Fig. 3B). In addition, amiloride-sensitive Na^+ influx as indicated by SBFI was found nearly absent in isolated granulosa cells from the cKO mice (Fig. 3C), which collectively suggested successful establishment of granulosa-specific knockout of ENaC in mice. The cKO mice were found overall healthy with no difference in body weight compared to the Ctrl ones. Female mice from the cKO model were then mated with wild-type male mice for fertility test, which showed that although the cKO mice achieved some successfully pregnancies with normal body weight pups (Supplementary Figure S2B), the averaged litter size over 3 consecutive pregnancies was significantly reduced in the cKO (4.1±0.9, $n=6$) compared to that of the Ctrl (6.9±0.5, $n=6$) mice (Fig. 3D), suggesting subfertility of the cKO female mice. The following ovarian morphological analysis showed that primary, secondary, antral and Graafian follicle counts were similar between the cKO and Ctrl (Fig. 3E). However, the number of corpus luteum was significantly reduced in the cKO (1.9±0.7, $n=10$) mice compared to the Ctrl (6.1±1.5, $n=6$) (Fig. 3E), suggesting problems in ovulation and/or luteinization in the cKO. We next monitored the estrus cycle of the mice for 20 days, which revealed that the estrus phase was significantly extended, and the diestrus phase was shortened in the cKO mice ($n=8$), as compared to either the Ctrl mice ($n=8$) or the Cre positive control (Cre-Ctrl, *Scnn1a*$^{wt/wt}$*Cyp19a1*$^{Cre+}$, $n=3$) mice at reproductive ages of 8 to 10 weeks old (Fig. 3F). The estrus ratio (proestrus/estrus versus metestrus/diestrus) was thus significantly increased in the cKO (Fig. 3F), suggesting the disturbance of estrus homeostasis and possibly problematic responses to gonadotrophins caused by granulosa knockout of ENaC.

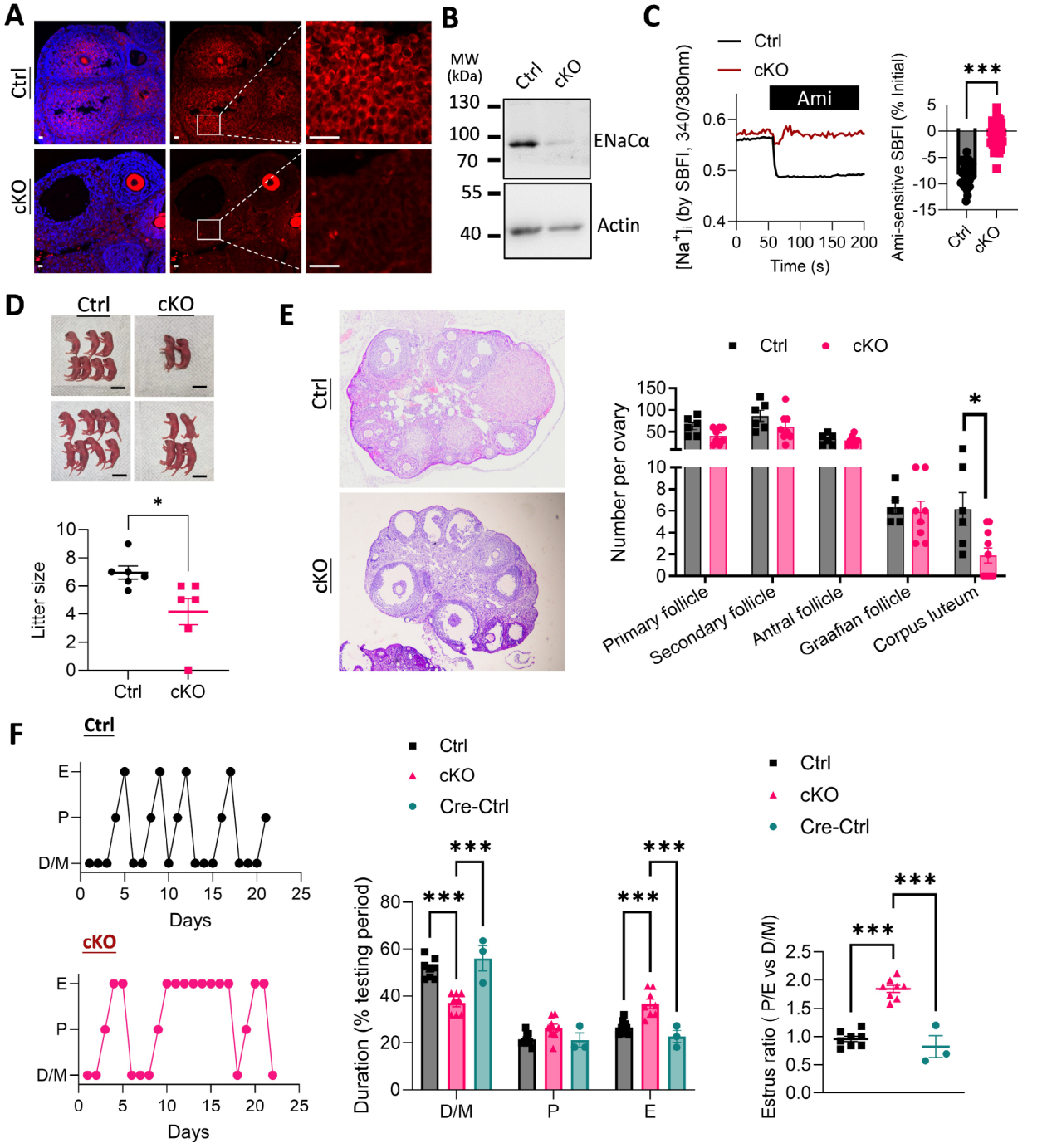

Fig. 3 Granulosa-cell specific knockout of ENaC disturbs estrus cycle and impairs female fertility in mice. (**A**) Representative images of immunofluorescence staining for ENaCα in ovarian tissues from a Cre-LoxP transgenic mouse model with ENaCα gene (*Scnn1a*) conditionally knocked out in ovarian granulosa cells (cKO, $Scnn1a^{fl/fl}Cyp19a1^{Cre+}$). Cre negative and *Scnn1a* floxed mice ($Scnn1a^{fl/fl}Cyp19a1^{Cre-}$) were used as the control (Ctrl). Scale bars, 20 μm. (**B**-**C**) Western blots for ENaCα (**B**) and SBFI measurement of $[Na^+]_i$ (**C**) in primary cultured granulosa cells from the Ctrl or cKO mice. Ami (1 μM) was added to calculate ENaC-mediated Na^+ movement. $n = 33–41$. $^{***}P < 0.001$ by Unpaired Student's t-test. (**D**) Representative photographs of newborn litters from the cKO or Ctrl pregnancies after crossing with wild-type males, with quantification of litter size. Data are averaged pup numbers of 3 consecutive pregnancies of each examined mouse. $n = 6$ mice. $^{*}P < 0.05$ by Unpaired Student's t-test. Scale bars, 10 mm. (**E**) Hematoxylin and eosin (H&E) staining of mouse ovarian tissue sections and counting (see methods) of follicles at different stages (i.e., primary, secondary, antral, graafian follicles) of folliculogenesis as well as corpus lutea in Ctrl and cKO mice. Data are numbers of follicles/corpus lutea per ovary. $n = 6$ (Ctrl), $n = 8–10$ (cKO) mice. $^{*}P < 0.05$ by Unpaired Student's t-test. (**F**) Tracking of different estrus cycle phases (D, P, E and M, determined by daily vaginal spear) for continuously 20 days in the cKO and Ctrl mice, and in Cre-positive wild-type *Scnn1a* mice ($Scnn1a^{wt/wt}Cyp19a1^{Cre+}$) as the Cre-control (Cre-Ctrl), with calculation of duration of phases and the estrus ratio (P/E versus D/M). $n = 8$ (Ctrl), 8 (cKO) and 3 (Cre-Ctrl). $^{***}P < 0.001$ by one-way ANOVA with post-hoc Tukey's test

Transcriptome analysis of granulosa cells with ENaC knockout

To further understand the granulosa changes in the cKO model, we conducted transcriptome analysis of the granulosa cells from the model by RNA sequencing (RNA-seq). To obtain synchronized granulosa cells in responding to gonadotrophins and avoid complex hypothalamus/pituitary feedback in vivo, we isolated granulosa cells from immature (25-day-old) cKO (*Scnn1a*$^{fl/fl}$*Cyp19a1*$^{Cre+}$) or Ctrl (*Scnn1a*$^{fl/fl}$*Cyp19a1*$^{Cre-}$) mice and treated the cultures with FSH (100 ng/mL, 48 h) and subsequently LH (100 ng/mL, 18 h) mimicking gonadotrophin stimulation in late folliculogenesis and ovulation. RNA-seq was then performed on these cells before and after the FSH/LH treatment, which detected a total of 17,855 genes. Among them, there were 224 differentially expressed genes (DEGs, $P<0.05$) between cKO and Ctrl (cKO versus Ctrl, Supplementary Figure S3A), and 435 DEGs after the FSH/LH treatment (cKO_FSH/LH versus Ctrl_FSH/LH, Supplementary Figure S3B). KEGG enrichment analysis of these DEGs revealed a number of pathways, especially in categories of *signal transduction* and *endocrine system*, were significantly altered in the cKO cells compared to the Ctrl (Supplementary Figure S3C). A known ENaC-related *aldosterone-regulated sodium reabsorption pathway* (KEGG Term ID: 04960) hit the highest enrichment ratio (0.18, $Q<0.01$) (Fig. 4A), confirming ENaC to be centrally affected in the cKO. Importantly, the *ovarian steroidogenesis pathway* (KEGG Term ID: 04913) was significantly varied between cKO_FSH/LH and Ctrl_FSH/LH groups with the enrichment ratio at 0.15 ($Q<0.0001$) (Fig. 4A). GO enrichment analysis consistently suggested significant changes in *steroid biosynthetic process* (GO:0006694, ratio at 0.13, $Q=0.0027$), *ovarian follicle development* (GO:0001541, ratio at 0.125, $Q=0.011$) and *response to estradiol* (GO:0032355, ratio at 0.093, $Q=0.0028$) between cKO_FSH/LH and Ctrl_FSH/LH groups (Fig. 4B). Further analysis using KEGG and GO databases revealed that 53 genes critical to ovarian steroidogenesis, oocyte maturation, ovulation and/or ovarian diseases were significantly changed in cKO versus Ctrl cells under FSH/LH treatment including *Lhcgr*, *Cyp19a1*, *Cyp17a1*, *Fshr* (Fig. 4C). The transcriptome analysis therefore suggested ENaC to be a critical factor to modulate granulosa responses to gonadotrophins.

ENaC contributes to Ca^{2+} mobilization in granulosa cells

We next asked how exactly ENaC regulates gonadotrophin signaling in granulosa cells. Since Na^+ influx through ENaC can depolarize membrane potential and open voltage-gated Ca^{2+} channels, we supposed Ca^{2+} signaling to be involved. Indeed, in the above KEGG/GO analysis, we found that 40 genes belonging to *Ca*$^{2+}$*binding* or *Ca*$^{2+}$*signaling* pathways were differently ($Q<0.05$) expressed between cKO and Ctrl cells after the FSH/LH treatment (Fig. 4D). We next used an independent granulosa cell model, KGN, to monitor intracellular Ca^{2+} activities through imaging with Fura-2, a Ca^{2+}-sensitive fluorescent dye. Interestingly, spontaneous Ca^{2+} oscillations/waves were observed in KGN cells, which were abolished by the removal of extracellular Ca^{2+}, suggesting them to be dependent largely on Ca^{2+} entry (Supplementary Figure S4). Such spontaneous Ca^{2+} oscillations were attenuated by amiloride (1 to 10 μM) in a dose-dependent manner (Fig. 5A). The addition of activator of ENaC, trypsin (20 μg/mL), evoked a Ca^{2+} increase on top of the spontaneous oscillations, which was blocked by pretreatment of the cells with amiloride (1 μM, Fig. 5B). Also, FSH (100 ng/mL) facilitated the Ca^{2+} waves, which were blocked by subsequent addition of amiloride (Fig. 5C). We then conducted stable knockdown of ENaCα using different designs of shRNAs, shENaCα-1 to -5 in KGN cells. As indicated by qPCR and western blot (Supplementary Figure S5A, Fig. 5D), cells treated with shENaCα-2 and 5 achieved considerable knockdown by about 60% compared to control cells treated with scrambled shRNAs (shNC), which were then used in the following experiments. Spontaneous Ca^{2+} oscillations were present in shNC-treated control cells, which were, however, found largely reduced in cells treated with shENaCα-2 or -5 (Fig. 5E-F). Besides, FSH-evoked Ca^{2+} responses were attenuated in the shENaCα-2/-5-treated cells compared to shNC-treated cells (Fig. 5F, Supplementary Figure S5B). Consistently, spontaneous and FSH-induced Ca^{2+} responses were both observed in primary mouse granulosa cells (Supplementary Figure S6), which were attenuated by amiloride (Supplementary Figure S6) and significantly smaller in cells from cKO mice (Fig. 5G), as compared to respective control cells. Since Ca^{2+} release from endoplasmic reticulum (ER) are known to associate with Ca^{2+} oscillations [30], we tested the capacity of ER as Ca^{2+} stores in these cells. Thapsigargin (1 μM), an inhibitor of the ER Ca^{2+} ATPase, depleted ER to induce an elevation of intracellular Ca^{2+} in KGN cells, which were indeed significantly smaller in shENaCα-2/-5 treated cells compared to that of shNC-treated KGN cells (Fig. 6A). Given these observations, we tested the expression of genes related to Ca^{2+} homeostasis in the cells including Ca^{2+} channels or Ca^{2+} modulators in KGN cells (Supplementary Figure S7, Fig. 6B-C). qPCR results identified that genes related to Ca^{2+} influx from extracellular compartment (Voltage-dependent L-type calcium subunits, Fig. 6B), Ca^{2+} release from intracellular Ca^{2+} stores (*ITPR1*, *ITPR2*, *ITPR3*, *MICU1* and *MICU2*, Fig. 6C), and Ca^{2+} modulators *CALHM5* and *S100A10* (Fig. 6C) were downregulated in shENaCα-2/-5-treated KGN cells, as compared to shNC-treated cells. It should be noted that related mouse genes

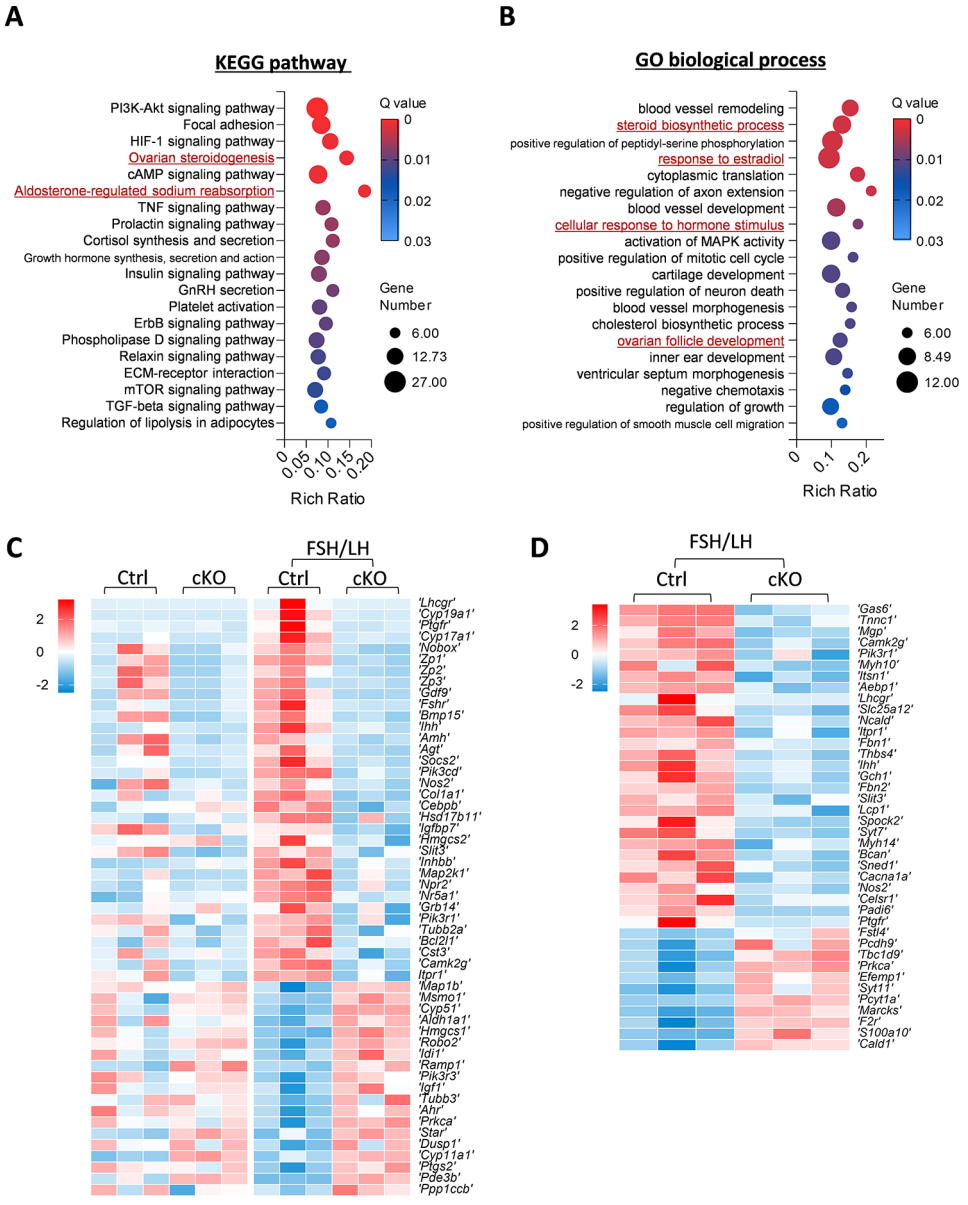

Fig. 4 Transcriptome analysis of granulosa cells with ENaC knockout. (**A**-**B**) RNA sequencing (RNA-seq) analysis of primary cultured granulosa cells from the cKO or Ctrl mice before and after treatment with FSH (100 ng/mL for 48 h) and subsequently LH (100 ng/mL for 18 h) revealed differentially expressed genes among the groups, which were further analyzed through enrichment assays using databases of KEGG pathway (**A**) and GO biological process (**B**). Data are presented as bubble charts with the bubble size indicating the number of genes, and color from blue to red, Q values from large to small. (**C**-**D**) Heatmaps showing RNA-seq detection of transcriptional changes of genes related to *ovarian steroidogenesis*, *oocyte maturation*, *ovulation and/or ovarian diseases* (**C**) and *Ca^{2+} binding or Ca^{2+} signaling pathways* (**D**) in primary granulosa cells from the cKO and Ctrl mice before and after the FSH/LH treatment. Blue to red colors in the heatmaps indicate row Z-scores from low to high

Cacna1a, *Itpr1*, *S100a10*, *Micu1* were also found to be significantly altered in the mouse granulosa cells from the cKO model (Fig. 4D). In addition, thapsigargin-evoked Ca^{2+} responses were substantially reduced in cKO cells compared to the Ctrl cells (Fig. 6D). Taken together, these results revealed a role of ENaC in modulating Ca^{2+} mobilization in granulosa cells.

ENaC modulates gonadotrophin signaling in both mouse and human granulosa cells

Given the above suggested association of ENaC with Ca^{2+} mobilization in granulosa cells, we further examined the role of ENaC in FSH/LH-stimulated granulosa cell responses for steroidogenesis and ovulation. We tested CREB, a Ca^{2+} and cAMP sensitive transcription factor known to mediate FSH- and LH-activated expression of genes essential to ovarian steroidogenesis and ovulation.

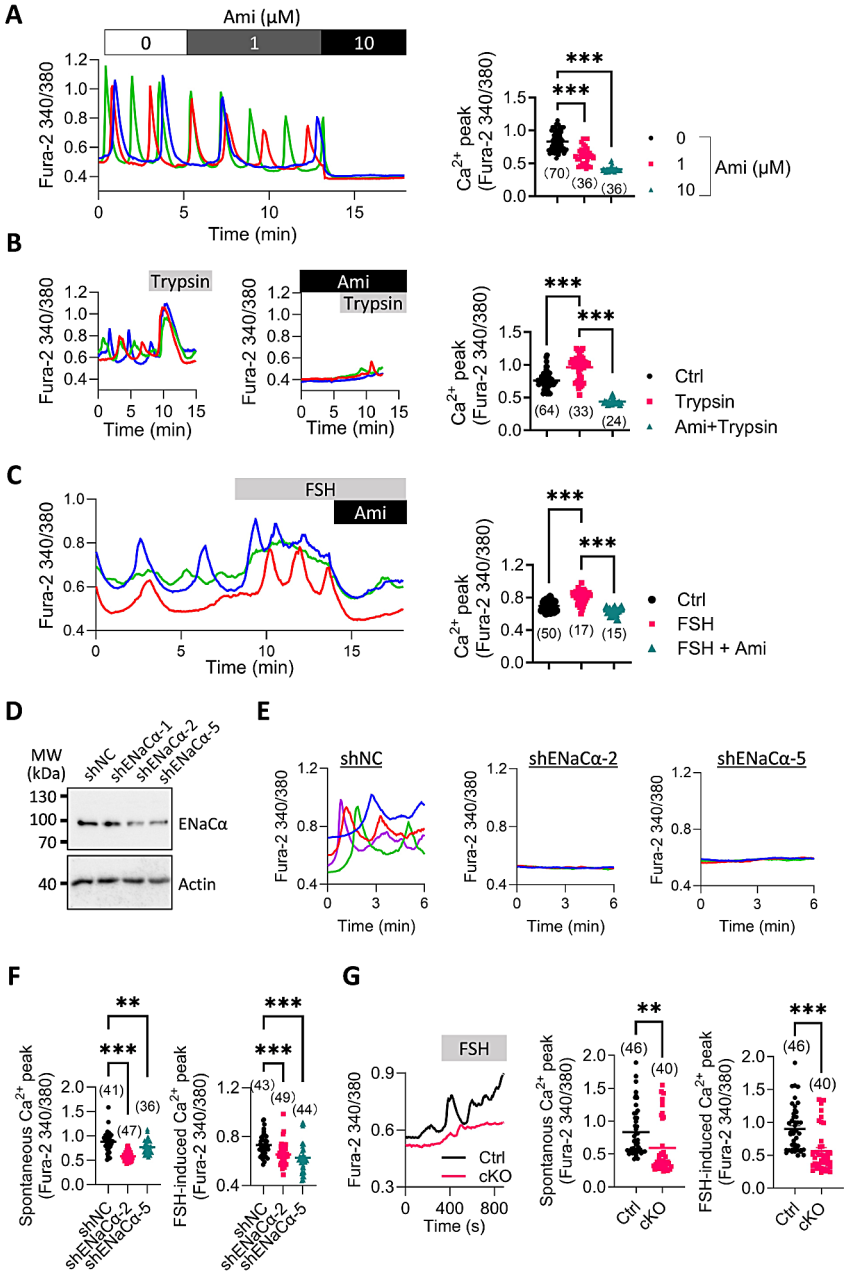

Fig. 5 ENaC contributes to Ca^{2+} mobilization in granulosa cells. (**A**) Fura-2 (a Ca^{2+} sensitive fluorescent dye) detection of spontaneous Ca^{2+} oscillations in KGN cells. *Left*: time-course traces of Fura-2 (ratio at 340/380 nm) in 3 representative KGN cells (in red, green and blue) before and after the addition of Ami (1 and 10 μM). *Right*: statistical analysis of maximal Fura-2 340/380 ratio (Ca^{2+} peak) under different conditions. n is shown for each group. ***$P < 0.001$ by one-way ANOVA with post-hoc Tukey's test. (**B**-**C**) Time-course changes in intracellular Ca^{2+} (indicated by Fura-2 ratio at 340/380) in 3 presentative KGN cells (in red, blue and green) in the presence or absence of trypsin (20 μg/mL), Ami (1 μM), or FSH (100 ng/mL), with corresponding statistical analysis. n is shown for each group. ***$P < 0.001$ by one-way ANOVA with post-hoc Tukey's test. (**D**) Western blots for ENaCα in KGN cells treated with different designs of shRNAs, shENaCα-1, -2 and -5 or scrambled shRNAs (shNC) as the control. (**E**-**F**) Representative (**E**) and statistical analysis (**F**) of Fura-2 measurement of spontaneous and FSH (100 ng/mL)-induced Ca^{2+} responses in KGN cells treated with shNC or shENaCα-2/-5. n is shown for each group. **$P < 0.01$, ***$P < 0.001$ by one-way ANOVA with post-hoc Tukey's test. (**G**) Fura-2 measurement of spontaneous and FSH (100 ng/mL)-induced Ca^{2+} responses in primary cultured granulosa cells from the Ctrl or cKO mice. n is shown for each group. **$P < 0.01$, ***$P < 0.001$ by Unpaired Student's t-test

Immunostaining for phosphorated CREB (pCREB, the activated form) in mouse ovarian tissues showed that in adult Ctrl mice, pCREB labeling was found in the nucleus of granulosa cells in antral follicles, but not in small follicles (e.g., secondary follicle) (Fig. 7A), consistent with its role in driving gonadotrophin-stimulated transcription of genes for late folliculogenesis and ovulation. Whereas, in cKO ovarian tissues, pCREB expression

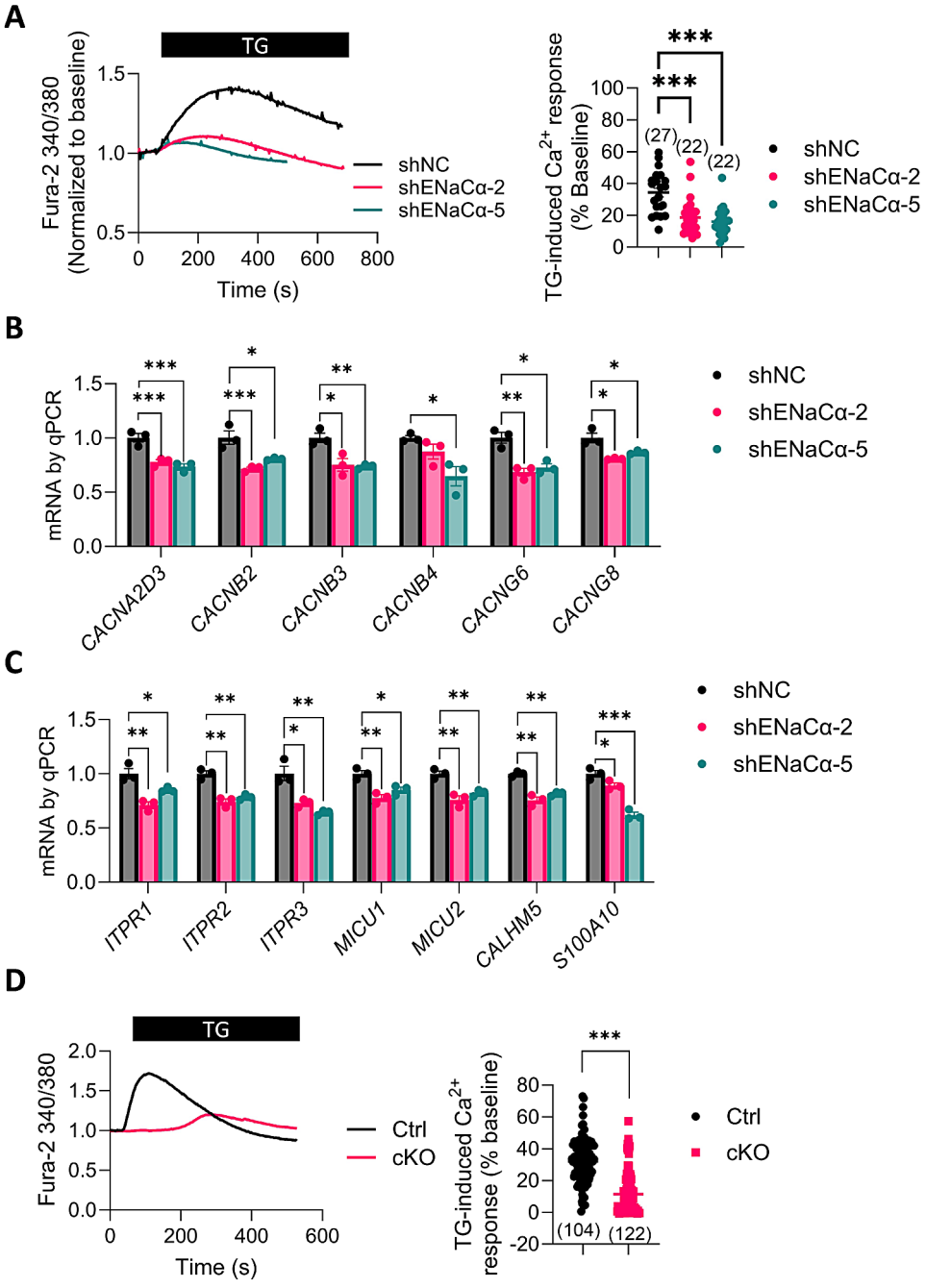

Fig. 6 ENaC contributes to the capacity of intracellular Ca^{2+} stores in granulosa cells. (**A**) Fura-2 measurement of intracellular Ca^{2+} levels in response to thapsigargin (TG, 1 μM), which depletes intracellular Ca^{2+} stores, in KGN cells treated with shENaCα-2/-5 or shNC as control. n is shown for each group. ***$P < 0.001$ by one-way ANOVA with post-hoc Tukey's test. (**B**-**C**) Quantitative PCR (qPCR) for genes related to Ca^{2+} influx from extracellular compartment (**B**), Ca^{2+} release from intracellular Ca^{2+} stores and Ca^{2+} modulators (**C**) in shNC or shENaCα-2/-5-treated KGN cells. $n = 3$. *$P < 0.05$, **$P < 0.01$, ***$P < 0.001$ by one-way with post-hoc Tukey's test. (**D**) Fura-2 measurement of intracellular Ca^{2+} levels in response to TG (1 μM) in primary granulosa cells from the Ctrl or cKO mice, with corresponding statistical analysis. n is shown for each group. ***$P < 0.001$ by Unpaired Student's t-test

in granulosa cells of large follicles was drastically diminished (Fig. 7A). We also tested CREB activation in mouse granulosa cell cultures. In Ctrl cells, the level of pCREB was elevated by FSH/LH (Fig. 7B). However, such pCREB activation in response to FSH/LH was found significantly impaired in cKO cells (Fig. 7B). In addition, qPCR detected that *Lhcgr*, *Cyp19a1* and *Fshr* genes were significantly upregulated by FSH/LH treatment in Ctrl cells, which were almost not responding to FSH/LH in cKO cells (Fig. 7C). Moreover, FSH/LH stimulated estradiol production were abolished in the cKO cells, compared to Ctrl cells (Fig. 7D). We also examined progesterone

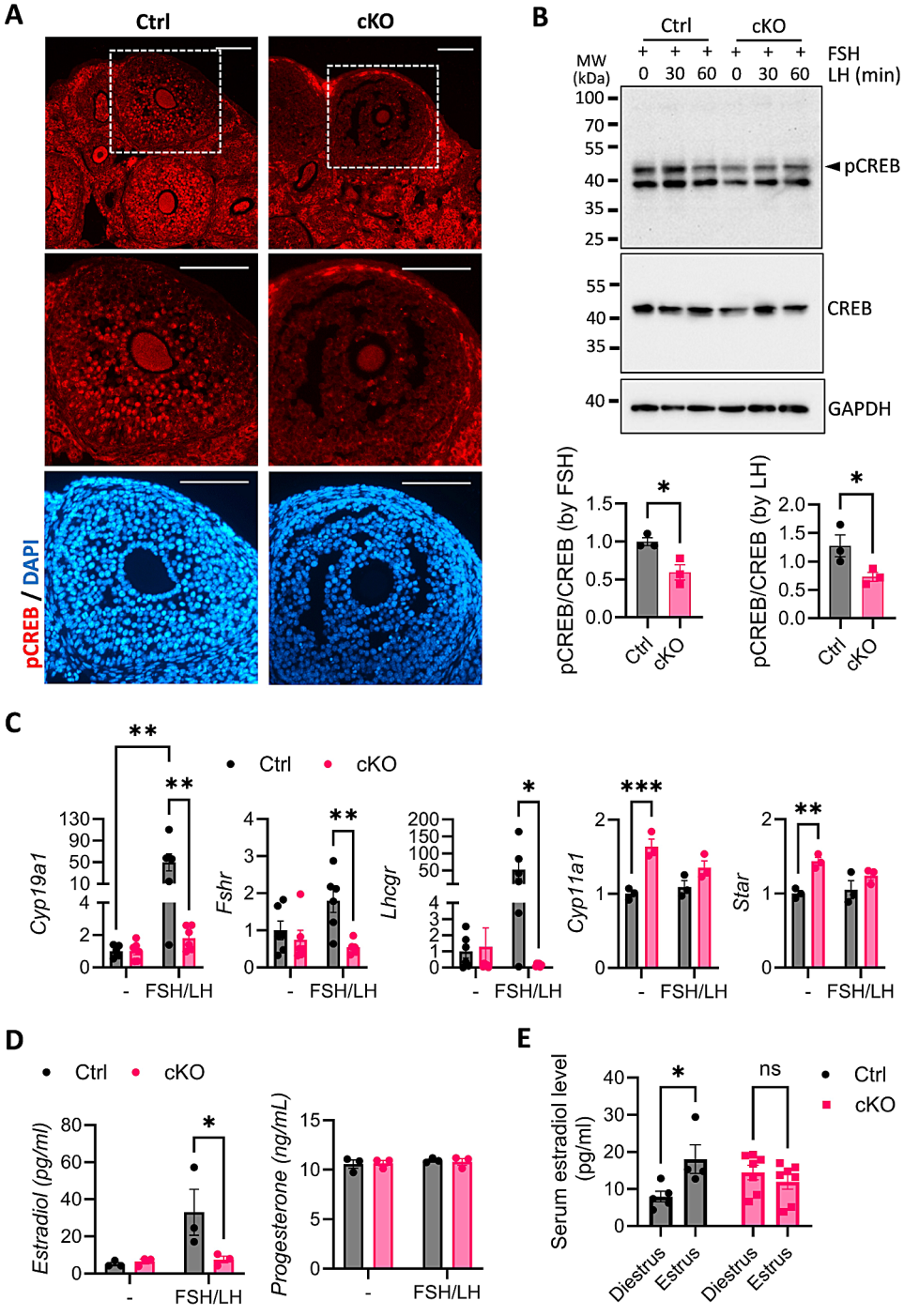

Fig. 7 ENaC modulates gonadotrophin signaling in mouse granulosa cells. (**A**) Representative images of immunofluorescence staining for phosphorated CREB (pCREB) in ovarian tissues from the Ctrl or cKO mice. The mice were injected with pregnant mare's serum gonadotropin (PMSG, 10 units/mouse, intraperitoneally) followed 48 h later with an injection of human chorionic gonadotropin (hCG, 10 units/mouse, intraperitoneally). Nuclei were labeled with DAPI. Scale bars, 100 μm. (**B**) Western blots for pCREB and CREB in primary cultured granulosa cells from the Ctrl or cKO mice, with corresponding statistical analysis. Cells were pretreated with FSH (100 ng/mL) for 48 h and subsequently LH (100 ng/mL) for 0, 30, 60 min. $n = 3$. $^{*}P < 0.05$ by Unpaired Student's t-test. (**C**-**D**) qPCR for genes related to ovarian steroidogenesis (**C**) and ELISA measurement of estradiol and progesterone level in cultured medium (**D**) of primary cultured granulosa cells from the cKO or Ctrl mice before and after treatment with FSH (100 ng/mL for 48 h) and subsequently LH (100 ng/mL for 18 h). $n = 3$–6. $^{*}P < 0.05$, $^{**}P < 0.01$, $^{***}P < 0.001$ by two-way ANOVA with post-hoc Tukey's test. (**E**) ELISA measurement of serum estradiol level in the Ctrl or cKO mice at day 1 of estrus and diestrus phases (determined by daily vaginal spear). $n = 5$–7. $^{*}P < 0.05$ by two-way ANOVA with post-hoc Tukey's test

production and found that although progesterone production associated genes *Cyp11a1* and *Star* genes were increased (about 1.5 folds) in cKO cells compared to the Ctrl cells (Fig. 7C), the progesterone level released from cells were similar among the groups (Fig. 7D). We went on to see if estrogen production in vivo was affected in the cKO mice. Results interestingly showed that in Ctrl mice, the serum estradiol level was elevated at day 1 of estrus phase compared to that at day 1 of diestrus (Fig. 7E). However, such estrus-related estrogen elevation was not seen in cKO mice (Fig. 7E). Besides, measuring serum FSH and LH levels in the mice showed that cKO mice exhibited a slightly higher FSH level than the Ctrl mice (Supplementary Figure S8). These hormonal results therefore explained the estrus cycle disturbance observed in the cKO mice. Given these observations in mouse models, we next tested the role of ENaC in gonadotrophin signaling in primary human granulosa cells isolated from women under IVF treatment (HGCs). Results showed that FSH or LH stimulated ENaCα protein expression in HGCs (Fig. 8A). Blocking of ENaC by amiloride (1 μM) or benzamil (1 μM, another inhibitor of ENaC) inhibited Ca^{2+} responses (Fig. 8B) and FSH-evoked CYP19A1 expression (Fig. 8C) in the HGCs. Taken together, these results suggested ENaC to modulate gonadotropin signaling in both mouse and human granulosa cells.

Discussion

In summary, the present study has demonstrated previously undefined expression and channel activity of ENaC in ovarian granulosa cells, which plays a role in modulating Ca^{2+} mobilization to promote FSH/LH-stimulated transcription changes and estrogen production in both mouse and human granulosa cells. Specific knockout of ENaC in granulosa cells results in disturbance of female cycle and reduced fertility in mice (Fig. 9).

Ovarian granulosa cells are not typical epithelial cells, although recent lineage studies suggest granulosa cells, in particular cortical granulosa cells, to be derived from ovarian surface epithelium [31]. The presently demonstrated granulosa expression of ENaC, a typical epithelial ion channel, may have been overlooked in the past. We detected primarily ENaCα expression in granulosa cells, while granulosa expression of ENaC β and γ subunits was found at a low level. We also searched an available human database, which similarly showed the detection of ENaCα subunit (*SCNN1A*) by single-cell RNA-seq in human

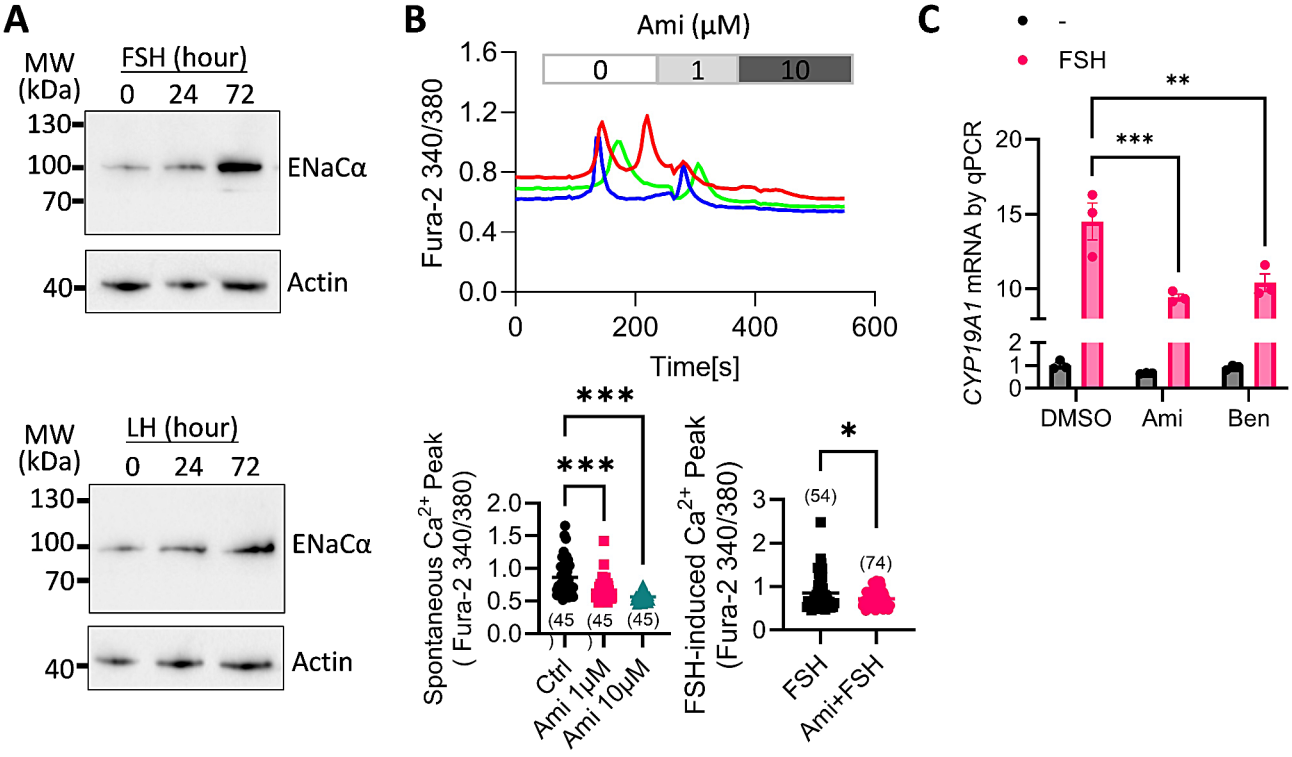

Fig. 8 ENaC modulates gonadotrophin signaling in human granulosa cells. (**A**) Western blots for ENaCα in HGCs treated with FSH (100 ng/mL) or LH (100 ng/mL) for 0, 24, 72 h. Cells were pretreated with FSH (100 ng/mL) for 48 h before LH was added. (**B**) Fura-2 measurement of intracellular Ca^{2+} levels in HGCs before (Ctrl) and after the addition of Ami (1 and 10 μM) or FSH (100 ng/mL) with/without pretreatment of Ami (10 μM), with corresponding statistical analysis. n is shown for each group. $^{*}P < 0.05$, $^{***}P < 0.001$ by one-way ANOVA with post-hoc Tukey's test. (**C**) qPCR for *CYP19A1* gene in HGCs treated with Ami (1 μM) or benzamil (1 μM, another inhibitor of ENaC) before and after treatment with FSH (100 ng/mL) for 48 h. DMSO was used as the control. $n = 3$. $^{**}P < 0.01$, $^{***}P < 0.001$ by two-way ANOVA with post-hoc Tukey's test

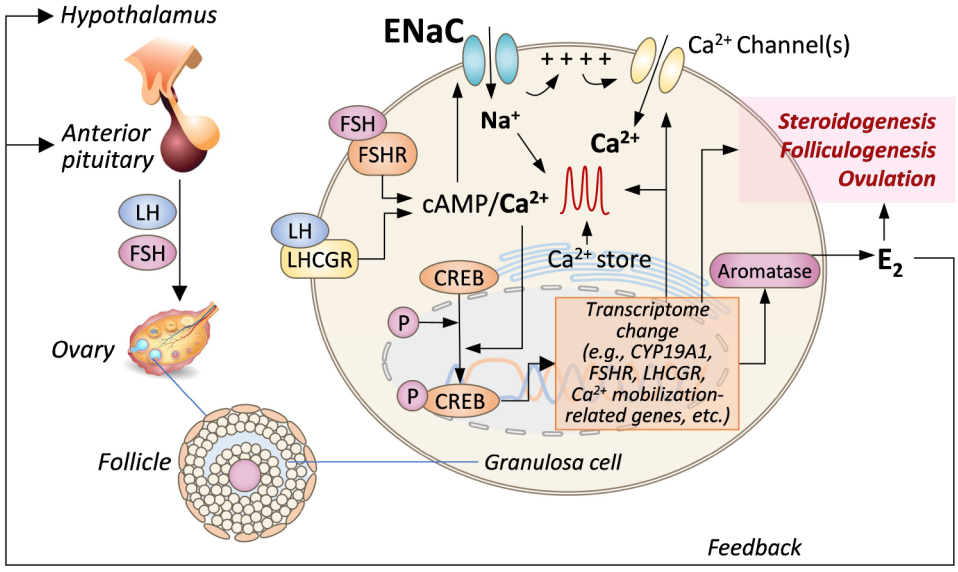

Fig. 9 Schematic model for the role of ENaC in granulosa cells. ENaC is expressed in ovarian granulosa cells to modulate Ca^{2+} mobilization including Ca^{2+} influx and Ca^{2+} release to promote FSH/LH-stimulated transcription changes and estrogen production for steroidogenesis, folliculogenesis and ovulation

ovarian granulosa populations but not β (*SCNN1B*) and γ (*SCNN1G*) [32]. Nevertheless, present patch-clamp or Na^+ imaging examination of human and mouse granulosa cells combined with the use of ENaC activator, inhibitor or knockout indicated ENaC channel activities in granulosa cells. ENaCα, therefore, is probably the primary contributor to the observed granulosa ENaC activities, since ENaCα subunits are known to assemble into channel pore in the membrane without β and γ [29].

The present study used different experimental models, including the mouse and human primary granulosa cultures, the KGN cell line and the transgenic mouse line. Although the models may have reported limitations, such as the lack of sensitivity of KGN cells to FSH/LH [33], data collected from these models are consistent to suggest a previously unknown role of ENaC in modulating gonadotropin signaling in granulosa cells. First, ovarian ENaCα was found to be upregulated at estrus phase in mice when gonadotrophins are largely released. In isolated mouse and/or human granulosa cells, FSH/LH increased ENaC expression and channel activity, which is consistent with the reported cAMP/Ca^{2+}-mediated enhancement of ENaC [34–36]. Second, the mice with granulosa knockout of ENaC exhibited phenotypes of defective responses to gonadotrophins, including 1) diminished granulosa CREB activation in large follicles, 2) failed estrogen elevation at early estrus phase, 3) reduced number of corpus luteum indicating impaired ovulation,4) extended estrus phase suggesting problematic transition into next cycle, and 5) reduced litter size and subfertility. Moreover, results on isolated mouse granulosa cells provided direct evidence that FSH/LH-induced granulosa transcriptome change and estrogen production is significantly impaired by ENaC knockout, indicating ENaC as a key factor in gonadotrophin signaling and thus ovarian steroidogenesis, late folliculogenesis and ovulation. Given the observed trypsin-activation of ENaC in granulosa cells, ENaC can be highly active at ovulation when ovarian serine proteases are reported to surge [37]. It should be noted that the cKO mouse model we adopted is driven by *Cyp19a1*. Although insufficiency and non-specificity of the Cre model was reported [38], our data suggested the Cre was successfully turned on to knockout ENaCα in granulosa cells in the ovary. *Cyp19a1* expression is known to be largely turned on only at late folliculogenesis, which is consistent with the present observations that only late development stage granulosa functions (i.e., steroidogenesis and ovulation) are affected in the cKO mice. However, whether ENaC is involved in early folliculogenesis or not will need more effective models (e.g., Cre-driven by early granulosa-specific genes) to confirm.

In the exploration of the mechanisms underlying ENaC's involvement in gonadotrophin signaling, we found that Ca^{2+} mobilization in granulosa cells at either the resting (i.e., spontaneous Ca^{2+} oscillations) or activated state (i.e., FSH-induced) is affected by ENaC inhibition, knockdown or knockout. Our data suggests ENaC to modulate Ca^{2+} mobilization in two folds. First, the action of ENaC could be quick and immediate, since pharmacological inhibition of ENaC quickly blocked Ca^{2+} increases. This is consistent with what we previously demonstrated in endometrial epithelial cells that ENaC-mediated Na^+ influx and hence depolarization can mobilize Ca^{2+} entry through voltage-gated Ca^{2+} channels [24]. In fact, voltage-gated Ca^{2+} and Na^+ channels were

reported to be present in granulosa cells [17–19], which is in line with the quick effect of ENaC-mediated depolarization on Ca^{2+} mobilization. Second, ENaC can play a long-term regulatory role to maintain Ca^{2+} mobilization as well. This is demonstrated using independent models, ENaC knockout in mouse granulosa cells and knockdown in KGN cells, which both showed the expression of Ca^{2+} signaling-associated genes to be affected by ENaC deficiency. Such a transcription shift of Ca^{2+}-related genes could be resulted from the immediate negative effect of ENaC-deficiency on Ca^{2+} signaling leading to a vicious cycle. Or, ENaC-mediated Na^+ influx is supposed to be coupled with Na^+/K^+ pumps which alters ATP consumption and overall metabolism of the cells [39]. In fact, we observed that the cKO granulosa cells were growing slightly slower than the Ctrl cells (Supplementary Figure S9). However, further study is needed to confirm the involvement of Na^+/K^+ pumps. Interestingly, we also noted that the expression of Ca^{2+} channel-modulating proteins, such as S100A10 [40], and proteins related to Ca^{2+} stores, such as ITPR1, MICU1, were affected by ENaC deficiency. Whether a mechanism through protein-protein interaction underlies ENaC regulation of Ca^{2+} channels or Ca^{2+} stores may be worth further investigation. Ca^{2+} increase is known as an upstream event for the activation/phosphorylation of CREB, as we previously reported in endometrial cells [24, 25, 27]. Given the reported importance of Ca^{2+} activities to steroidogenesis, oocyte maturation and ovulation [13, 14, 41–43], the presently demonstrated regulation of Ca^{2+} mobilization by ENaC in granulosa cells provides new insights into the understanding ovarian physiological events.

It should be noted that although definitive data were achieved from mouse models presently, our results from human granulosa cells collected during IVF suggest a consistent role of ENaC in regulating FSH/LH signaling, for which we believe our findings to have clinical implications too. Although the mutation of ENaC genes is found to be rare in humans [44], cases of ENaC loss-of-function mutation or downregulation/abnormality in humans were correlated to female subfertility or miscarriage [23, 45]. In a study on women with different diary Na^+ levels showed that, compared to higher Na^+ intake, lower Na^+ intake was found associated with higher FSH and LH levels as well as an increased risk of anovulation [36], which is in line with present findings suggesting defective Na^+ channel in relation to disturbed female cycle. It is also interesting to note that cystic fibrosis transmembrane conductance regulator (CFTR), a closely interacting protein of ENaC [46, 47], has been known to be expressed in granulosa cells to enhance FSH-stimulated aromatase expression and estrogen production, defect of which is associated with polycystic ovarian syndrome [48]. Therefore, the presently demonstrated role of ENaC in ovarian granulosa cells may shed light on the understanding of idiopathic ovarian disorders or female infertility/subfertility. It is worth studying ENaC, either its expression or functional activities, as well as its associated proteins, in women with related ovarian disorders in the future. Additionally, in the current ART, extensive hormonal stimulation still poses a main concern [12]. Granulosa ENaC or environmental/dietary Na^+ might be a factor to be considered in hormonal management in ART. Moreover, new methods for in vitro oocyte maturation (IVM) are being developed to avoid ovarian hyperstimulation or aim for hormone-free ART [12]. Given the essential role of granulosa/cumulus cells in the survival of oocytes in vitro [49], it will be interesting to study whether granulosa ENaC could be important for providing an appropriate environment for oocyte maturation and embryo development in IVF technology in the future.

Materials and methods

Human subjects

Women under ART treatment at Prince of Wales Hospital, Hong Kong were recruited. All procedures were approved by Joint Chinese University of Hong Kong-New Territories East Cluster Clinical Research Ethics Committee (No. CT-2020-0339) and Hong Kong Polytechnic University (No. HSEARS202000317006-02). Written consents were obtained from all participants. General information about the participants is shown in Supplementary Table 1. Women with ovarian problems were excluded from the present study. IVF protocols were used as previously reported [50]. All participants were subjected to ovarian stimulation by either recombinant FSH or human menopausal gonadotrophins with doses ranging from 150 to 450 IU per day. Upon the presence of three or more follicles ≥ 16 mm in diameter under continuous ultrasound monitor, participants were given 5000 IU of hCG. Granulosa cells were collected from ovulatory follicles by transvaginal follicular aspiration 36 h after the hCG administration.

Animals

C57BL/6 mice were purchased from Centralized Animal Facilities (CAF), Hong Kong Polytechnic University and maintained at CAF in ventilated cases in a temperature (25℃)-controlled room with a 12-hour light-dark cycle,food and water *ad libitum*. All animal procedures were approved by Animal Subjects Ethics Sub-committee of Hong Kong Polytechnic University (No.20-21/151-BME-R-GRF and No. 22-23/449-BME-R-GRF). The *Scnn1a* floxed transgenic C57BL/6 mouse line (*Scnn1a*$^{fl/fl}$) was constructed in GemPharmtech Co., Ltd. (Jiangsu, China). Two loxP sequences (5'-ATA ACT TCG TAT AGC ATA CAT TAT ACG AAG TTA T-3') were inserted to flank the exon 2 of *Scnn1a* gene

(ENSMUST00000081440.13) by CRISPR/Cas9. Another transgenic C57BL/6 line containing *Cyp19a1*-driven Cre was kindly provided by Professor Xu Ying at Soochow University [51]. *Scnn1a* conditional knockout mice (*Scnn1a*$^{fl/fl}$*Cyp19a1*$^{Cre+}$) were generated by crossing the two lines. Fertility tests were done in the female mice by crossing with wild-type male mice, started at 2 months old, for continuously 90 days. Phases of the estrus cycle in adult (8 to12-week-old) mice were determined by vaginal cytology as we previously reported [52].

RNA extraction, reverse transcription and quantitative PCR

Total RNA of mouse ovarian tissues or cells was extracted using TRIzol reagent (Invitrogen, 15596026) following the manufacturer's instructions. 1 μg total RNA was transcribed reversely to cDNA using the High-Capacity cDNA Reverse Transcription kit (Invitrogen, 4368814). After reverse transcription, 1 μL of the cDNA of each sample was amplified in a 10 μL reaction system containing the SYBR Green Premix Ex Taq™ Mix (Takara, RR420A) and primers (Supplementary Table 2) using a real-time PCR system (Bio-Rad, CFX96). *GAPDH* or *Gapdh* was used as the internal control. Data were calculated by the $2^{-\Delta\Delta Ct}$ method.

Immunofluorescence

Mouse ovarian tissues were fixed with 4% paraformaldehyde, treated with 30% sucrose in PBS, embedded in optimal cutting temperature compound and cryo-sectioned into 5 μm sections by a cryotome (Cryostar NX70 Cryostat). Sections were rehydrated in PBS for 5 min before heated by a microwave in the Tris-EDTA buffer (10 mM Tris Base, 1 mM EDTA solution, 0.05% Tween 20, pH 9.0) for 20 min for antigen retrieval. After cooling down to room temperature, the sections were further treated with 1% SDS for 4 min, rinsed with PBS before incubated with 1% bovine serum albumin (BSA) in PBS for 15 min to block non-specific bindings. Primary antibodies (Supplementary Table 3) were used for incubation at 4℃ overnight and followed with fluorophore-conjugated secondary antibodies (Supplementary Table 4). Nuclei were labeled with DAPI (Vector lab, H-1800). Images were taken by a fluorescence microscope (Eclipse Ti2, Nikon, Japan) or a confocal microscope (Leica TCS SPE).

Histology and Immunohistochemistry

Mouse ovaries were fixed with 4% paraformaldehyde at 4℃ overnight. After dehydration by ethanol and xylene, tissues were embedded in paraffin and cut into 5 μm sections by a microtome (Leica RM2235). Sections were subject to hematoxylin and eosin staining for immunohistochemistry analysis. Briefly, the sections were deparaffinized by xylene and rehydrated in a series of ethanol solutions. Hematoxylin (Sigma, HHS32) and eosin Y (Sigma, 230251) were used. To label ENaCα, ovarian sections were quenched in 3% H_2O_2 in methanol for 20 min before heated in an acidic buffer (10 mM Sodium Citrate, 0.05% Tween 20, pH 6.0) or the above mentioned Tris-EDTA buffer at 65℃ for 20 min for antigen retrieval. After blocking in 1% BSA in PBS, primary antibody (Supplementary Table 3) was applied for incubation at 4℃ overnight. HRP-conjugated secondary antibodies (Supplementary Table 4) were applied next day followed with a DAB kit (Abcam, ab64238) . Nuclei were counterstained with hematoxylin.

Follicle and corpus luteum counting

Paraffin-embedded intact mouse ovaries were serially cut into 5 μm sections. To count primary, secondary and antral follicles, every 10th section from the serial sectioning was collected for hematoxylin and eosin staining and morphological assessment. The follicular stages (primary, secondary, antral and Graafian follicles) were determined by Pedersen and Peters morphological criteria [53]. Only the follicles with the presence of oocyte nucleus were counted to avoid double counting. Raw numbers from such counting were multiplied by the correction factor, 10, to estimate the follicle number per ovary. To count large Graafian follicles and corpus lutea, all sections spanning the entire ovary were carefully examined.

Cell culture

Human granulosa cells were obtained and cultured as previously reported [54]. Briefly, after dissecting the oocytes out for IVF, the remaining cells in follicular fluid were collected and centrifuged at 200 g for 10 min. Supernatant was removed and cell pellets were washed with PBS and subsequently treated with a red blood cell lysis buffer to eliminate red blood cells. Cells were cultured in Dulbecco's Modified Eagle Medium F-12 (DMEM/F12, Gibco,12400016) supplemented with 10% fetal bovine serum (FBS, Gibco, 10270106), 100 units/mL of penicillin and 100 μg/mL of streptomycin (Gibco, 15140122) in a 5% CO_2 incubator at 37℃.

Primary mouse granulosa cells were isolated and cultured as previously reported [48]. Briefly, ovaries were dissected from 25-day-old female mice, rinsed with PBS, and then placed in culture medium containing DMEM/F-12 supplemented with 10% FBS, 100 units/mL of penicillin and 100 μg/mL of streptomycin. Granulosa cells were released from the ovarian tissues by puncturing large preantral follicles using 25-gauge needles, which were afterwards centrifuged at 400 g for 5 min and cultured in a 5% CO_2 incubator at 37℃.

The KGN cell line was a generous gift from Prof Zhang Dan at Zhejiang University, and maintained using DMEM/F-12 in 10% FBS.

Gene knockdown

shRNAs targeting human *SCNN1A* gene (shENaC-1: 5'-CCG GCC AGA ACA AAT CGG ACT GCT TCT CGA GAA GCA GTC CGA TTT GTT CTG GTT TTT G-3'; shENaC-2: 5'-CCG GCG ATG TAT GGA AAC TGC TAT ACT CGA GTA TAG CAG TTT CCA TAC ATC GTT TTT G-3'; shENaC-3: 5'-CCG GGA ACA ATT ACA CCG TCA ACA ACT CGA GTT GTT GAC GGT GTA ATT GTT CTT TTT G-3'; shENaC-4: 5'-CCG GCC CGG AAA TTA AAG AGG AGC TCT CGA GAG CTC CTC TTT AAT TTC CGG GTT TTT G-3'; shENaC-5: 5'-CCG GCG CAG AGC AGA ATG ACT TCA TCT CGA GAT GAA GTC ATT CTG CTC TGC GTT TTT G-3') and scrambled shRNAs (shNC: 5'- TTC TCC GAA CGT GTC ACG TTT C-3') were purchased from Sigma-Aldrich. To package the shRNAs into lentivirus, envelope vector pMD2.G (Addgene, #12259) and packaging vectors psPAX2 (Addgene, #12260) together with the shRNAs were transfected into 293FT cells using lipofectamine 2000 in OptiMEM medium (Invitrogen). The packaged virus was harvested 48 and 72 h afterwards and used for transfection into KGN cells with polybrene (6 μg/mL, Sigma, TR-1003). The cells were subsequently screened with puromycin (1 μg/mL, Gibco, A1113802) for 14 days to achieve a stable knockdown of ENaCα in the KGN cells for further experiments.

Western blot

Cells or ovarian tissues were lysed with RIPA buffer (150 mM NaCl, 50 mM Tris-Cl, 1% NP-40, 0.5% DOC and 0.1% SDS, pH 7.5) containing 1% protease and phosphatase inhibitor cocktail (Thermo Scientific, 78443) for 30 min on ice. Supernatant was collected as total protein after centrifugation at 14,000 rpm for 30 min at 4 °C. Equal amounts of protein were separated by SDS-polyacrylamide (SDS-PAGE) gel electrophoresis and then electroblotted onto equilibrated nitrocellulose membrane with semi-dry transfer system. After blocking with 5% nonfat milk, the membranes were immunodetected for target proteins. Primary antibodies and their usages are listed in Supplementary Table 3. The protein bands were detected with HRP-conjugated antibodies (Supplementary Table 4) and visualized by the chemiluminescence (ECL) assay (GE Healthcare) using the ChemiDoc MP Imaging System (Bio-Rad). Signals were quantified by ImageJ software.

Whole-cell patch-clamp

Cells were seeded in the 35 mm culture dishes for 24 h before the patch-clamp experiments. A micropipette puller (P-97, Sutter Instrument Co., USA) was used to pull glass pipettes. The resistance of pipettes was 5–7 mΩ after filled with pipette solution. Whole-cell currents were recorded by a data acquisition system (DigiData 1322 A, Axon Instruments) and an amplifier (Axopatch-200B, Axon Instruments, Foster City, CA USA). The command voltages were controlled by a computer equipped with pClamp Version 9 software. A bath solution containing (in mM): Na-gluconate (145), KCl (2.7), $CaCl_2$ (1.8), $MgCl_2$ (2), glucose (5.5), HEPES (10) (pH 7.4) was used. Pipettes were filled with a solution containing (in mM): K-gluconate (135), KCl (10), NaCl (6), HEPES (10), $MgCl_2$ (2) (pH 7.2).

Na^+ and Ca^{2+} imaging

Cells were seeded on coverslips for two days before the experiments. Cells were washed with a bath solution (Margo-Ringer solution) containing (in mM) NaCl (130), KCl (5), $CaCl_2$ (2.5), $MgCl_2$ (1), glucose (10), HEPES (20) (pH 7.4) before incubated with Pluronic™ F-127 (1.25 μM, Invitrogen, P3000MP) and SBFI-AM (10 μM, Invitrogen, S1263, for Na^+ imaging) or Fura2-AM (2.5 μM, Invitrogen, F1221, for Ca^{2+} imaging) in the bath solution for 30 min at 37℃. Afterwards, residual dyes were washed out and cells on coverslips were equilibrated in the bath solution for 10 min before mounted in a mini chamber and placed onto a fluorescence microscope (Eclipse Ti2, Nikon, Japan). Fluorescence signals were excited by the dual wavelength at 340 and 380 nm with emission collected at 510 nm. Pictures were taken every 3–5 s.

ELISA

ELISA kits for estradiol (Cayman, 501890), progesterone (Cayman, 582601), FSH (Cusabio, E06871m) and LH (Cusabio, E12770m) were used according to the manufacture' instructions. When measuring estradiol, mouse blood samples were collected on the first day of estrus and the first day of diestrus respectively, pre-treated with methanol before assay according to the ELISA manufacturer's instructions. For the culture-medium sample, granulosa cells were treated with testosterone (100 nM, Sigma, T1500) overnight.

RNA sequencing and data analysis

RNAs were extracted from Ctrl and cKO mouse granulosa cells before and after treatment with FSH (100 ng/mL, 48 h, Sigma, F4021) and subsequently LH (100 ng/mL, 18 h, Sigma, L6420) using RNeasy Mini Kit (Qiagen, 74104) and sent to BGI Corporation for quality check before RNA sequencing was done. FPKM (fragments per kilobase of transcript sequence per millions base pairs sequenced) was used to estimate gene expression levels. Enrichment analysis was done by mapping all identified DEGs with each entry of Gene Ontology database (http://www.geneontology.org/) or KEGG database (http://www.genome.jp/kegg/) with hypergeometric tests. Q value (corrected P value) $\leq$ 0.05 was used as the threshold. Dr.

Tom, an online analyzing platform provided by BGI Corporation was used.

MTT assay

Primary granulosa cells derived from the cKO and Ctrl mice were seeded onto a 96-well plate at a density of 2000 cells per well. Cells were treated with MTT labeling reagent (0.5 mg/mL, Invitrogen, M6494) at 37℃ for 2 h before DMSO was added each day for 7 days. The absorbance was read at 595 nm by a microplate reader (Labexim Products LEDETECT 96).

Statistics

Paired or Unpaired Student's t-test was used for comparisons between two groups. One-way ANOVA was used for comparisons of more than two groups. Two-way ANOVA was used when two independent variables were involved. P values <0.05 were considered as statistically significant. GraphPad Prism 10.0 was used for statistic analysis.

Supplementary Information

The online version contains supplementary material available at https://doi.org/10.1186/s12964-024-01778-5.

Supplementary Material 1

Acknowledgements

The work was supported in part by the General Research Fund (No. 82071599) from the National Natural Science Foundation of China, General Research Fund (No.15106423 and No.15102622) and Areas of Excellence Scheme of Hong Kong (No. AoE/M-402/20) from The Research Grant Council of Hong Kong, and Seed Fund by Joint Research Centre for Biosensing and Precision Theranostics, Hong Kong Polytechnic University. We thank Dr Chen Xiaoyan, Dr Guo Xi and Dr Chan Yiu Leung for their help in collecting clinical samples. We thank University Research Facility in Life Sciences (ULS) at Hong Kong Polytechnic University for equipment and technical support.

Author contributions

Conception: Y.C.R.; Experiments and/or data analysis: X.M., R.X., J.C., S.W., P.H., Y.W., Y.Q., W.D., X.C., and Y.C.R.; Intellectual input: H.C., and J.G., Clinical materials and consultancy: T.C.L.; Manuscript writing: Y.C.R with contribution from other authors.

Data availability

No datasets were generated or analysed during the current study.

Declarations

Competing interests

The authors declare no competing interests.

Received: 23 May 2024 / Accepted: 6 August 2024
Published online: 14 August 2024

References

1. Li R, Albertini DF. The road to maturation: somatic cell interaction and self-organization of the mammalian oocyte. Nat Rev Mol Cell Biol. 2013;14:141–52. https://doi.org/10.1038/nrm3531.
2. Sanchez F, Smitz J. Molecular control of oogenesis. Biochim Biophys Acta. 2012;1822:1896–912. https://doi.org/10.1016/j.bbadis.2012.05.013.
3. Duffy DM, Ko C, Jo M, Brannstrom M, Curry TE. Ovulation: parallels with inflammatory processes. Endocr Rev. 2019;40:369–416. https://doi.org/10.1210/er.2018-00075.
4. Stocco C. Aromatase expression in the ovary: hormonal and molecular regulation. Steroids. 2008;73:473–87. https://doi.org/10.1016/j.steroids.2008.01.017.
5. Payne AH, Hales DB. Overview of steroidogenic enzymes in the pathway from cholesterol to active steroid hormones. Endocr Rev. 2004;25:947–70. https://doi.org/10.1210/er.2003-0030.
6. Chakravarthi VP, Ratri A, Masumi S, Borosha S, Ghosh S, Christenson LK, Roby KF, Wolfe MW, Rumi MAK. Granulosa cell genes that regulate ovarian follicle development beyond the antral stage: the role of estrogen receptor beta. Mol Cell Endocrinol. 2021;528:111212. https://doi.org/10.1016/j.mce.2021.111212.
7. Bao X, Yan D, Yang J, Zhang Z, Yuan B. Role of ERbeta in the ovary and ovary related diseases. Gene. 2024;927:148678. https://doi.org/10.1016/j.gene.2024.148678.
8. Richards JS, Russell DL, Robker RL, Dajee M, Alliston TN. Molecular mechanisms of ovulation and luteinization. Mol Cell Endocrinol. 1998;145:47–54. https://doi.org/10.1016/s0303-7207(98)00168-3.
9. Uda M, Ottolenghi C, Crisponi L, Garcia JE, Deiana M, Kimber W, Forabosco A, Cao A, Schlessinger D, Pilia G. Foxl2 disruption causes mouse ovarian failure by pervasive blockage of follicle development. Hum Mol Genet. 2004;13:1171–81. https://doi.org/10.1093/hmg/ddh124.
10. Pangas SA, Jorgez CJ, Tran M, Agno J, Li X, Brown CW, Kumar TR, Matzuk MM. Intraovarian activins are required for female fertility. Mol Endocrinol. 2007;21:2458–71. https://doi.org/10.1210/me.2007.
11. Duan CC, Li C, He YC, Xu JJ, Shi CY, Hu HT, Su YF, Chen L, Tan YJ, Liu ZW, et al. Oocyte exposure to supraphysiological estradiol during ovarian stimulation increased the risk of adverse perinatal outcomes after frozen-thawed embryo transfer: a retrospective cohort study. J Dev Orig Health Dis. 2020;11:392–402. https://doi.org/10.1017/S2040174419000679.
12. Gilchrist RB, Ho TM, De Vos M, Sanchez F, Romero S, Ledger WL, Anckaert E, Vuong LN, Smitz J. A fresh start for IVM: capacitating the oocyte for development using pre-IVM. Hum Reprod Update. 2024;30:3–25. https://doi.org/10.1093/humupd/dmad023.
13. Flores JA, Veldhuis JD, Leong DA. Follicle-stimulating hormone evokes an increase in intracellular free calcium ion concentrations in single ovarian (granulosa) cells. Endocrinology. 1990;127:3172–9. https://doi.org/10.1210/endo-127-6-3172.
14. Paul S, Kundu S, Pramanick K, Bandyopadhyay A, Mukherjee D. Regulation of ovarian steroidogenesis in vitro by gonadotropin in common carp Cyprinus carpio: interaction between calcium- and adenylate cyclase-dependent pathways and involvement of ERK signaling cascade. J Mol Endocrinol. 2010;45:207–18. https://doi.org/10.1677/JME-10-0061.
15. Egbert JR, Fahey PG, Reimer J, Owen CM, Evsikov AV, Nikolaev VO, Griesbeck O, Ray RS, Tolias AS, Jaffe LA. Follicle-stimulating hormone and luteinizing hormone increase Ca2 + in the granulosa cells of mouse ovarian follicles. Biol Reprod. 2019;101:433–44.
16. Squires PE, Lee PS, Yuen BH, Leung PC, Buchan AM. Mechanisms involved in ATP-evoked Ca2 + oscillations in isolated human granulosa-luteal cells. Cell Calcium. 1997;21:365–74. https://doi.org/10.1016/s0143-4160(97)90030-0.
17. Agoston A, Kunz L, Krieger A, Mayerhofer A. Two types of calcium channels in human ovarian endocrine cells: involvement in steroidogenesis. J Clin Endocrinol Metab. 2004;89:4503–12. https://doi.org/10.1210/jc.2003-032219.
18. Bahena-Alvarez D, Millan-Aldaco D, Rincon-Heredia R, Escamilla-Avila N, Hernandez-Cruz A. Expression of voltage-gated ca(2+) channels, Insp(3)rs, and RyRs in the immature mouse ovary. J Ovarian Res. 2022;15:85. https://doi.org/10.1186/s13048-022-01015-y.
19. Bulling A, Berg FD, Berg U, Duffy DM, Stouffer RL, Ojeda SR, Gratzl M, Mayerhofer A. Identification of an ovarian voltage-activated Na+-channel type: hints to involvement in luteolysis. Mol Endocrinol. 2000;14:1064–74. https://doi.org/10.1210/mend.14.7.0481.
20. Garty H, Palmer LG. Epithelial sodium channels: function, structure, and regulation. Physiol Rev. 1997;77:359–96. https://doi.org/10.1152/physrev.1997.77.2.359.
21. Hummler E, Barker P, Gatzy J, Beermann F, Verdumo C, Schmidt A, Boucher R, Rossier BC. Early death due to defective neonatal lung liquid clearance in alpha-ENaC-deficient mice. Nat Genet. 1996;12:325–8. https://doi.org/10.1038/ng0396-325.

22. Boggula V, Hanukoglu I, Sagiv R, Enuka Y, Hanukoglu A. Identification of epithelial Sodium Channel (ENaC) in endometrial Pipelle Biopsy samples. Horm Res Paediat. 2018;90:121–121.
23. Boggula VR, Hanukoglu I, Sagiv R, Enuka Y, Hanukoglu A. Expression of the epithelial sodium channel (ENaC) in the endometrium - implications for fertility in a patient with pseudohypoaldosteronism. J Steroid Biochem Mol Biol. 2018;183:137–41. https://doi.org/10.1016/j.jsbmb.2018.06.007.
24. Ruan YC, Guo JH, Liu X, Zhang R, Tsang LL, Dong JD, Chen H, Yu MK, Jiang X, Zhang XH, et al. Activation of the epithelial na + channel triggers prostaglandin E(2) release and production required for embryo implantation. Nat Med. 2012;18:1112–7. https://doi.org/10.1038/nm.2771.
25. Sun X, Ruan YC, Guo J, Chen H, Tsang LL, Zhang X, Jiang X, Chan HC. Regulation of miR-101/miR-199a-3p by the epithelial sodium channel during embryo implantation: involvement of CREB phosphorylation. Reproduction. 2014;148:559–68. https://doi.org/10.1530/REP-14-0386.
26. Ruan YC, Chen H, Chan HC. Ion channels in the endometrium: regulation of endometrial receptivity and embryo implantation. Hum Reprod Update. 2014;20:517–29. https://doi.org/10.1093/humupd/dmu006.
27. Sun X, Guo JH, Zhang D, Chen JJ, Lin WY, Huang Y, Chen H, Huang WQ, Liu Y, Tsang LL, et al. Activation of the epithelial sodium channel (ENaC) leads to cytokine profile shift to pro-inflammatory in labor. EMBO Mol Med. 2018;10. https://doi.org/10.15252/emmm.201808868.
28. Kim K, Wactawski-Wende J, Michels KA, Schliep KC, Plowden TC, Chaljub EN, Mumford SL. Dietary minerals, reproductive hormone levels and sporadic anovulation: associations in healthy women with regular menstrual cycles. Br J Nutr. 2018;120:81–9. https://doi.org/10.1017/S0007114518000818.
29. Canessa CM, Schild L, Buell G, Thorens B, Gautschi I, Horisberger JD, Rossier BC. Amiloride-sensitive epithelial na + channel is made of three homologous subunits. Nature. 1994;367:463–7. https://doi.org/10.1038/367463a0.
30. Li YX, Keizer J, Stojilkovic SS, Rinzel J. Ca2 + excitability of the ER membrane: an explanation for IP3-induced Ca2 + oscillations. Am J Physiol. 1995;269:C1079–1092. https://doi.org/10.1152/ajpcell.1995.269.5.C1079.
31. Rotgers E, Jorgensen A, Yao HH. At the crossroads of fate-somatic cell lineage specification in the fetal gonad. Endocr Rev. 2018;39:739–59. https://doi.org/10.1210/er.2018-00010.
32. Karlsson M, Zhang C, Méar L, Zhong W, Digre A, Katona B, Sjöstedt E, Butler L, Odeberg J, Dusart P. A single–cell type transcriptomics map of human tissues. Sci Adv. 2021;7:eabh2169.
33. Havelock JC, Rainey WE, Carr BR. Ovarian granulosa cell lines. Mol Cell Endocrinol. 2004;228:67–78. https://doi.org/10.1016/j.mce.2004.04.018.
34. Snyder PM, Olson DR, Kabra R, Zhou R, Steines JC. cAMP and serum and glucocorticoid-inducible kinase (SGK) regulate the epithelial na + channel through convergent phosphorylation of Nedd4-2. J Biol Chem. 2004;279:45753–8.
35. Mustafa SB, Castro R, Falck AJ, Petershack JA, Henson BM, Mendoza YM, Choudary A, Seidner SR. Protein kinase A and mitogen-activated protein kinase pathways mediate cAMP induction of α-Epithelial na + channels (α-ENaC). J Cell Physiol. 2008;215:101–10.
36. Morris RG, Schafer JA. cAMP increases density of ENaC subunits in the apical membrane of MDCK cells in direct proportion to amiloride-sensitive na + transport. J Gen Physiol. 2002;120:71–85.
37. Ohnishi J, Ohnishi E, Shibuya H, Takahashi T. Functions for proteinases in the ovulatory process. Biochim Biophys Acta. 2005;1751:95–109. https://doi.org/10.1016/j.bbapap.2005.05.002.
38. Fan HY, Liu Z, Paquet M, Wang J, Lydon JP, DeMayo FJ, Richards JS. Cell type-specific targeted mutations of Kras and Pten document proliferation arrest in granulosa cells versus oncogenic insult to ovarian surface epithelial cells. Cancer Res. 2009;69:6463–72. https://doi.org/10.1158/0008-5472.CAN-08-3363.
39. Feraille E, Dizin E. Coordinated control of ENaC and Na+,K+-ATPase in Renal Collecting Duct. J Am Soc Nephrol. 2016;27:2554–63. https://doi.org/10.1681/ASN.2016020124.
40. Saiki Y, Horii A. Multiple functions of S100A10, an important cancer promoter. Pathol Int. 2019;69:629–36. https://doi.org/10.1111/pin.12861.
41. Carroll J, Swann K, Whittingham D, Whitaker M. Spatiotemporal dynamics of intracellular [Ca2+]i oscillations during the growth and meiotic maturation of mouse oocytes. Development. 1994;120:3507–17. https://doi.org/10.1242/dev.120.12.3507.
42. Miao YL, Stein P, Jefferson WN, Padilla-Banks E, Williams CJ. Calcium influx-mediated signaling is required for complete mouse egg activation. Proc Natl Acad Sci U S A. 2012;109:4169–74. https://doi.org/10.1073/pnas.1112333109.
43. Stricker SA. Comparative biology of calcium signaling during fertilization and egg activation in animals. Dev Biol. 1999;211:157–76. https://doi.org/10.1006/dbio.1999.9340.
44. Hanukoglu I, Hanukoglu A. Epithelial sodium channel (ENaC) family: phylogeny, structure–function, tissue distribution, and associated inherited diseases. Gene. 2016;579:95–132.
45. Wang S, He G, Yang Y, Liu Y, Diao R, Sheng K, Liu X, Xu W. Reduced expression of Enac in Placenta tissues of patients with severe preeclampsia is related to compromised trophoblastic cell migration and invasion during pregnancy. PLoS ONE. 2013;8:e72153. https://doi.org/10.1371/journal.pone.0072153.
46. Horisberger JD. ENaC-CFTR interactions: the role of electrical coupling of ion fluxes explored in an epithelial cell model. Pflugers Arch. 2003;445:522–8. https://doi.org/10.1007/s00424-002-0956-0.
47. Wuchu F, Ma X, Que Y, Chen J, Ruan YC. Biphasic regulation of CFTR expression by ENaC in epithelial cells: the involvement of ca(2+)-modulated cAMP production. Front Cell Dev Biol. 2022;10:781762. https://doi.org/10.3389/fcell.2022.781762.
48. Chen H, Guo JH, Lu YC, Ding GL, Yu MK, Tsang LL, Fok KL, Liu XM, Zhang XH, Chung YW, et al. Impaired CFTR-dependent amplification of FSH-stimulated estrogen production in cystic fibrosis and PCOS. J Clin Endocrinol Metab. 2012;97:923–32. https://doi.org/10.1210/jc.2011-1363.
49. Richani D, Dunning KR, Thompson JG, Gilchrist RB. Metabolic co-dependence of the oocyte and cumulus cells: essential role in determining oocyte developmental competence. Hum Reprod Update. 2021;27:27–47. https://doi.org/10.1093/humupd/dmaa043.
50. Saravelos SH, Wong AWY, Chan CPS, Kong GWS, Cheung LP, Chung CHS, Chung JPW, Li TC. Assessment of the embryo flash position and migration with 3D ultrasound within 60 min of embryo transfer. Hum Reprod. 2016;31:591–6. https://doi.org/10.1093/humrep/dev343.
51. Dong Z, Huang M, Liu Z, Xie P, Dong Y, Wu X, Qu Z, Shen B, Huang X, Zhang T, et al. Focused screening of mitochondrial metabolism reveals a crucial role for a tumor suppressor Hbp1 in ovarian reserve. Cell Death Differ. 2016;23:1602–14. https://doi.org/10.1038/cdd.2016.47.
52. Wu Y, Que Y, Chen J, Sun L, Guo J, Ruan YC. CFTR modulates hypothalamic neuron excitability to maintain female cycle. Int J Mol Sci. 2023;24. https://doi.org/10.3390/ijms241612572.
53. Pedersen T, Peters H. Proposal for a classification of oocytes and follicles in the mouse ovary. J Reprod Fertil. 1968;17:555–7. https://doi.org/10.1530/jrf.0.0170555.
54. Yang F, Ruan YC, Yang YJ, Wang K, Liang SS, Han YB, Teng XM, Yang JZ. Follicular hyperandrogenism downregulates aromatase in luteinized granulosa cells in polycystic ovary syndrome women. Reproduction. 2015;150:289–96. https://doi.org/10.1530/REP-15-0044.

Publisher's Note